Long-Lived Charge-Separated States in ZnS/Na-MOR Zeolite upon trans-Stilbene Adsorption

Pedro Henrique Morais Andrade, Matthieu Hureau, Anne-Sophie Mamede, Pascale Massiani, Alexandre Legrand, Alain Moissette

Long-Lived Charge Separate States in ZnS/Na-MOR Zeolite upon Trans-Stilbene Adsorption

Pedro H. M. Andrade[1], Matthieu Hureau[1], Anne-Sophie Mamede[2], Pascale Massiani[3], Alexandre Legrand[2,*], Alain Moissette[1,*]

(1) Laboratoire de Spectroscopie pour les Interactions, la Réactivité et l'Environnement (LASIRE), UMR-CNRS 8516, Université de Lille – Sciences et Technologies, 59655 - Villeneuve d'Ascq, France.

(2) Unité de Catalyse et Chimie du Solide (UCCS), Univ. Lille, CNRS, Centrale Lille, Univ. Artois, UMR 8181, F-59000 Lille, France

(3) Laboratoire de Réactivité de Surface, UMR 7197 Sorbonne Université-CNRS, 4 place Jussieu 75005 Paris, France

* corresponding authors

alexandre.legrand@univ-lille.fr – ORCID: 0000-0002-7975-9348

alain.moissette@univ-lille.fr – ORCID: 0000-0003-2713-5143

M. Hureau – ORCID: 0000-0001-8163-6614

P.H.M Andrade – ORCID: 0000-0002-8264-1818

ABSTRACT

Electron transfer (ET) processes are of fundamental importance in many photochemical processes of biological and chemical systems. Here, semiconductors nanoparticles of ZnS (as electron relay) and trans-stilbene molecules (*t*-St) (as electron donor), both confined within the porous volume of mordenite (MOR), are combined to mimic photosynthetic process. ZnS nanoparticles were synthesized by cationic exchange between the counterion of the zeolite and ZnS precursors in solution. The characterization of ZnS/Na-MOR composite was performed by powder X-Ray Diffraction (XRD), diffuse reflectance UV-Vis spectroscopy, X-Ray Photoelectron Spectroscopy (XPS), and Transmission Electron Microscopy (TEM) coupled with Energy Dispersive X-Ray Spectroscopy (EDS). These complementary techniques highlight the successful formation of ZnS nanoparticles at the surface of Na-MOR. The electron transfer mechanisms taking place after the incorporation and photoionization of *t*-St molecules was evaluated using diffuse reflectance UV-Vis spectroscopy. The results show the formation of long-lived *t*-$St^{\bullet+}$@ZnS/Na-$MOR^{\bullet-}$ charge separate states (lifetime = 18 min; k = 0.0553 min^{-1}) whose stability is linked to the nature of the new charge compensating cation, and to the close proximity of the ZnS nanoparticles, which are probably located within the zeolite framework. Indeed, the augmentation of the transient species lifetime was attributed to an electron transfer from the *t*-St molecule towards the ZnS conduction band.

KEYWORDS: Mordenite; ZnS; Semiconductor; trans-stilbene; adsorption; electron transfer; charge separate state; Spectroscopy.

1. INTRODUCTION

The ability to induce and temporarily maintain charge separate states (CSS) is essential for the functioning of natural and artificial light energy harvesting systems. Zeolites as host porous materials for photochromic guest molecules have been reported to generate long-lived charge separate state.[1–4] The charge separate states formed can be generated experimentally by photolysis, radiolysis, or spontaneously simply by the contact between the molecules with the zeolites. Together with the reduced mobility of the trapped molecules, parameters such as the nature of the charge compensating cations, the pore size diameter of the host and the aluminium content in the zeolite framework can limit the radical recombination.[5,6] Even if the formation of separate charge states with good efficiency and a long lifetime is an important advance, a crucial step for the system to be applicable lies in the possibility of capturing the electrons after their initial ejection and their trapping in the inorganic network. However, a particular problem then arises since zeolites are aluminosilicate materials, a well-known insulator. A promising solution could be to transfer the generated electrons to the conduction band of a conductive material placed near the chromophore.

Titanium oxide (TiO_2), a typical n-type semiconductor, has been previously deposited as nanocluster on the surface of mordenite (MOR) zeolite in order to investigate the transfer of electrons, produced by spontaneous or photo-induced ionization of a guest molecule (*trans*-stilbene, *t*-St) occluded in the pores, towards the conduction band of the semi-conductors.[7] Strongly stabilized *t*-$St^{\bullet+}$ radicals were detected in the TiO_2-MOR samples whereas such species were never detected in pristine mordenite. It was proposed that the proximity of TiO_2 with the formed t-$St^{\bullet+}$ radicals induces the stabilization of the radical through capture of the ejected electron by the semi-conductor. Nevertheless, titanium was found to be mainly located at the external surface of the zeolite grains, in the form of highly dispersed and/or aggregated anatase and could result to a non-optimal configuration for an efficient charge transfer process.

ZnS is a well-known semiconductor material that finds applications in several fields such as sensitizers, photovoltaic solar cells, flat screen technologies, or photocatalysis.[8] Several studies have evaluated the capacity of ZnS to form clusters with dimensions comparable to the exciton Bohr radius, also known as quantum dots.[9,10] Therefore, in order to tailor the size and morphology of the nanoclusters and, consequently, their optical and electronic properties, the “ship in a bottle” synthesis of clusters in micro or

mesoporous host has been developed.[11–14] In this case, the channel diameter limits the clusters' size and geometry in 1, 2 or 3 dimensions. In addition to non-linear optical applications, the quantum size effect can be used to carry out electron-transfer processes that are usually inaccessible to the bulk semiconductor [15].

In this work, we propose a new route to accommodate ZnS nanoparticles in the channels of mordenite-type zeolite. ZnS nanoparticles were synthesized within mordenite-type zeolite starting from Na_2S and $ZnCl_2$ precursors. The ionic exchange process between the charge compensating cations of the zeolite and the ZnS precursors is expected to favour the formation of intra-zeolitic ZnS clusters. The *t*-St guest molecule was absorbed within the host ZnS/Na-MOR composite. The guest molecule was chosen for its relatively low ionization energy in gas phase (7.65 eV) and the host for its unique structure that represents a good compromise between ionization yield, transient species lifetimes, and intermediary pore diameters. The electron transfer mechanisms taking place after the incorporation and photoionization of *t*-St molecules within ZnS/Na-MOR composite was evaluated using diffuse reflectance UV-vis spectroscopy.

2. MATERIALS AND METHODS

Syntheses: The formation of the ZnS nanoclusters to be incorporated into the MOR was achieved through an ion exchange between the counterbalancing cation of the zeolite and the ZnS precursor. First, $ZnCl_2$ (Alfa Cesar, anhydrous 98%, 0.12 mol, 16.36 g) was previously degassed under argon for three hours. Then, the powder was added into a 120 mL aqueous suspension containing NH_4–MOR (Zeolyst International, 8 g). The mixture was kept under magnetic stirring under argon atmosphere for 24 h at room temperature to allow the ion exchange. Later, the product was collected by filtration, washed with deionized water, and dried overnight at 323 K. The procedure was repeated at least three times to get an optimum cation exchange. Afterward, 80 mL of Na_2S (Sigma Aldrich) was added into the final solution containing the exchanged zeolite to induce the formation of ZnS. Finally, the sample denoted ZnS/Na-MOR was recovered by filtration and calcined at 723 K for 12 h under argon. At the end of these exchanges, the extra-framework

NH_4^+ charge balancing cations are assumed to be completely replaced by sodium ions. Pristine ZnS (99.99 %) was obtained from Sigma Aldrich and use for comparative purposes.

Trans-stilbene sorption: 1.0 g of calcinated ZnS/Na-MOR sample was mixed under argon with 25 mg of *t*-St, which corresponds to one *t*-St molecule per unit cell of MOR (2.5 wt.%). The powders were transferred under dry argon into a quartz glass Suprasil cell and kept at room temperature until complete sorption.

X-ray diffraction: powder X-ray Diffraction (PXRD) patterns of the different compounds were registered at room temperature (RT) using a Bruker D8 Advance A25 diffractometer with Bragg-Brentano geometry (θ-2θ mode) equipped with a LynxEye detector with CuK_α radiation. The 2θ scans were performed in the 5-50° range, with a step size of 0.02° and a speed of 0.6°/min.

Transmission electronic microscopy: The ZnS particle morphologies and dispersions information were evaluated by TEM, combined with energy dispersive X-ray spectroscopy (EDS) and high-resolution transmission electron microscopy (HRTEM) analysis. The images were obtained using a JEOL JEM 2011 instrument operated with an acceleration voltage of 200 kV. Zeolites samples were prepared on Leica's microtome to obtain thin sections of 70 nm.

Infrared spectroscopy: FTIR was performed on a Nicolet Magna 860 apparatus equipped with a liquid-nitrogen-cooled MCT detector (Mid-IR) with the suitable beam splitter. The spectra were recorded with a 2 cm^{-1} resolution using 1024 scans.

Diffuse reflectance UV-vis spectroscopy: The UV−vis experiments were carried out on a Varian Cary 6000i spectrometer using an external integrating sphere (DRA-1800) to study the powder samples through diffuse reflectance. The spectra were recorded in the 200−900 nm spectral range with a resolution of 1 nm. The diffuse reflectance spectra were plotted using the Kubelka−Munk function.

Band gap evaluation: The apparent band gap energy (E_g) of the materials was evaluated using the data obtained by diffuse reflectance UV-vis spectroscopy. E_g was assessed by plotting the so-called Kubelka-Munk function [$(F(R)h\nu)^n$] against the photon energy ($h\nu$), where h is the Planck constant (4.14×10^{-15} eV.s), and ν is the photon frequency (Hz). The index n is a function of the electron transition observed in the examined material – e.g., indirect allowed transition (n = 1/2), direct allowed transition (n = 2), indirect forbidden transition (n = 3), or direct forbidden transition (n = 2/3). F(R) was calculated by Equation (1), where R is the reflectance (%) assessed by UV-vis spectroscopy.

$$\boldsymbol{F(R) = \frac{(1-R)^2}{2R}} \qquad (\mathbf{1})$$

X-ray photoelectron spectroscopy: XPS analyses were performed using a Kratos Analytical AXIS UltraDLD spectrometer. A monochromatized aluminium source (Al K_α = 1486.6 eV) with an X-ray beam diameter around 1 mm used for excitation. The analyser was operated in constant pass energy of 40 eV using an analysis area of approximately 700 μm x 300 μm. Charge compensation was applied to overcome the charging effect occurring during the analysis. The C 1s (285.0 eV) binding energy (BE) was used as internal reference. The spectrometer BE scale was initially calibrated against the Ag $3d_{5/2}$ (368.2 eV) level. Pressure was in the 10^{-10} Torr range during the experiments. Quantification and simulation of the experimental peaks were carried out using the CasaXPS software. Quantification considered a non-linear Shirley background subtraction.

Photoexcitation: The excitation pulses at 300 nm (7 to 8 ns, 10 mJ) were applied using a 20 Hz Panther EX OPO tuneable laser (Continuum, GSI group).

3. RESULTS AND DISCUSSION

3.1 CHARACTERIZATION OF THE PRISTINE MATERIALS

Powder XRD was conducted for evaluating the incorporation of ZnS into the MOR, as well as the stability of the zeolite structure after the cation exchange and calcination (Figure 1). The patterns of the ZnS/Na-MOR material is similar to that of the raw zeolite, indicating that the NH_4-MOR did not undergo any amorphization or significant structural transformation. Moreover, after the cation exchange procedure, two additional diffraction peaks were detected at 28.52 and 47.96 º. These signals are ascribed to the presence of ZnS and can be related either to the plans (002) and (110) of its hexagonal phase (wurtzite), or to the (111) and (220) of its cubic phase (sphalerite).[16,17] However, due to the absence of the two main peaks of wurtzite in the samples' XRD pattern, it is possible to infer that sphalerite phase was formed in this case. Moreover, from the widening of the diffraction peaks that is usually characteristic of nanocrystals, ZnS was found to crystalize as nanoparticles of around 3 nm, as determined from the Scherrer equation.[18–20] It is worth mentioning that this value works as an approximation in which the crystallites have a normal particle size distribution centred around 3 nm.[21,22]

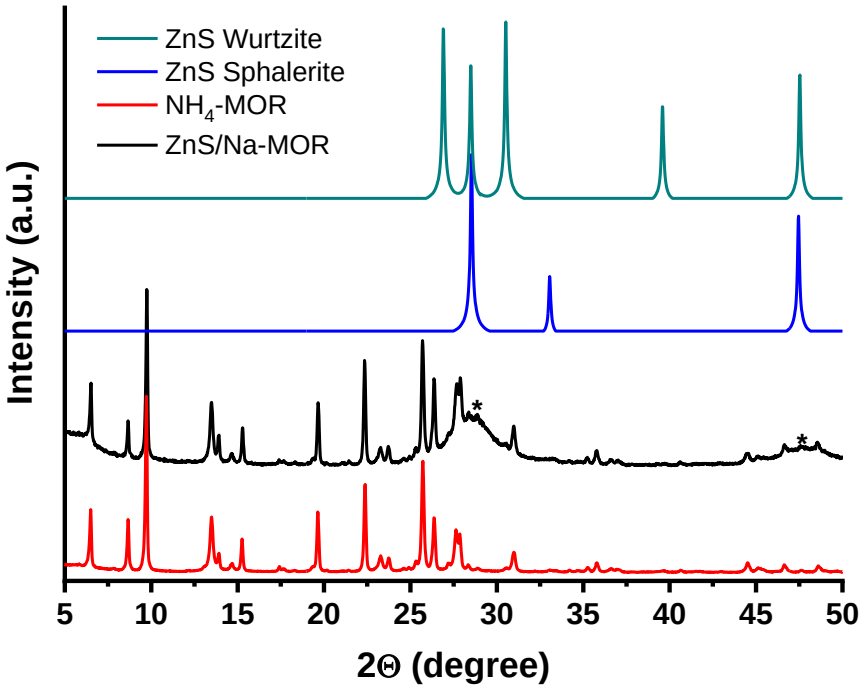

Figure 1: Powder XRD of NH_4–MOR (black), ZnS/Na-MOR (red) and simulated pattern of sphalerite (blue) and wurtzite (cyan) phases of ZnS. The (*) indicates the two peaks related to ZnS at 28.52 and 47.96°. $\lambda_{CuK\alpha}$ = 1.5406 Å.

To verify the size and morphology of the ZnS nanoparticles as well as their distribution and chemical composition in ZnS/Na-MOR, TEM images were obtained together with HRTEM and EDS analysis (Figure 2). Ultramicrotomy cross-section images of ZnS/Na-MOR show ZnS nanoclusters formed at the surface of the zeolite in the form of aggregate as confirmed by EDS chemical analysis (Figure 2a inset). The high-resolution microphotography of ZnS clusters shows particles of diameter around 3.0 nm (Figure 2b), in accord with the value obtained using the Scherrer formula on the ZnS/Na-MOR XRD diffractogram. The particle size observed is larger than the main pore channels of the mordenite (6.5 Å) that indicate a partial migration and aggregation of ZnS from the zeolite channels to the crystallite surface. In addition, the ordered contrast pattern that can be observed in the ZnS nanoparticles is clearly visible in the fast Fourier transform of the image (Figure 2b inset). The SAED provides three circular spots centred at 3.05, 1.9 and 1.7 Å, which are related to the (111), (220), and (311) reticular planes characteristic of ZnS sphalerite phase.[23,24]

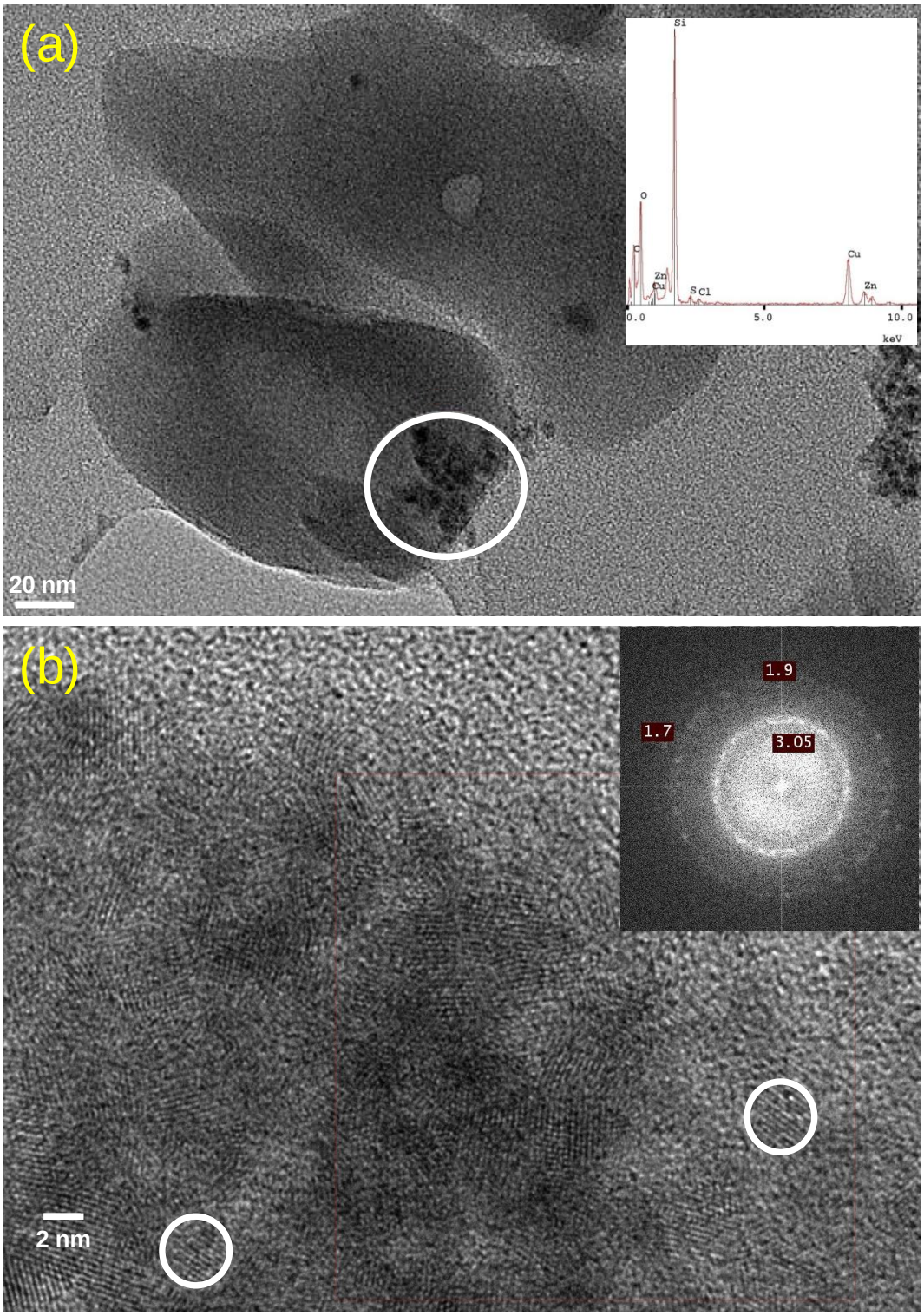

Figure 2: (a) TEM images of ZnS/Na-MOR showing aglomerates of ZnS nanoparticles. Inset: EDS spectrum of the white circle region. (b) HRTEM micrograph of ZnS/Na-MOR showing ZnS nanoparticles of about 3.0 nm. Inset: fast-Fourier transform of the particles (circled zones).

Diffuse reflectance UV-Vis spectroscopy was conducted to evaluate the electronic properties of ZnS nanoparticles within the MOR framework compared to bulk ZnS and pristine MOR (Figure 3a). The bulk ZnS semiconductor exhibited a broad absorption band with a maximum of absorption (λ_{max}) around 326 nm,

which is characteristic of the exciton (electron-hole) transition in the sphalerite phase of ZnS.[25] On the other hand, the spectrum of the NH_4-MOR exhibits a main absorption band centred around 275 nm which is ascribed to charge-transfer complexes between the metal cations and the oxygen/nitrogen atoms of the zeolite.[26,27] On the other hand, the spectrum of the ZnS/Na-MOR composite shows a blueshift regarding its absorption band edge when compared to those of both bulk ZnS and NH_4-MOR compounds. This feature is tentatively attributed to a quantum size effect and is ascribed to a decrease in the ZnS particle size, as observed for several semiconductors.[28–30]

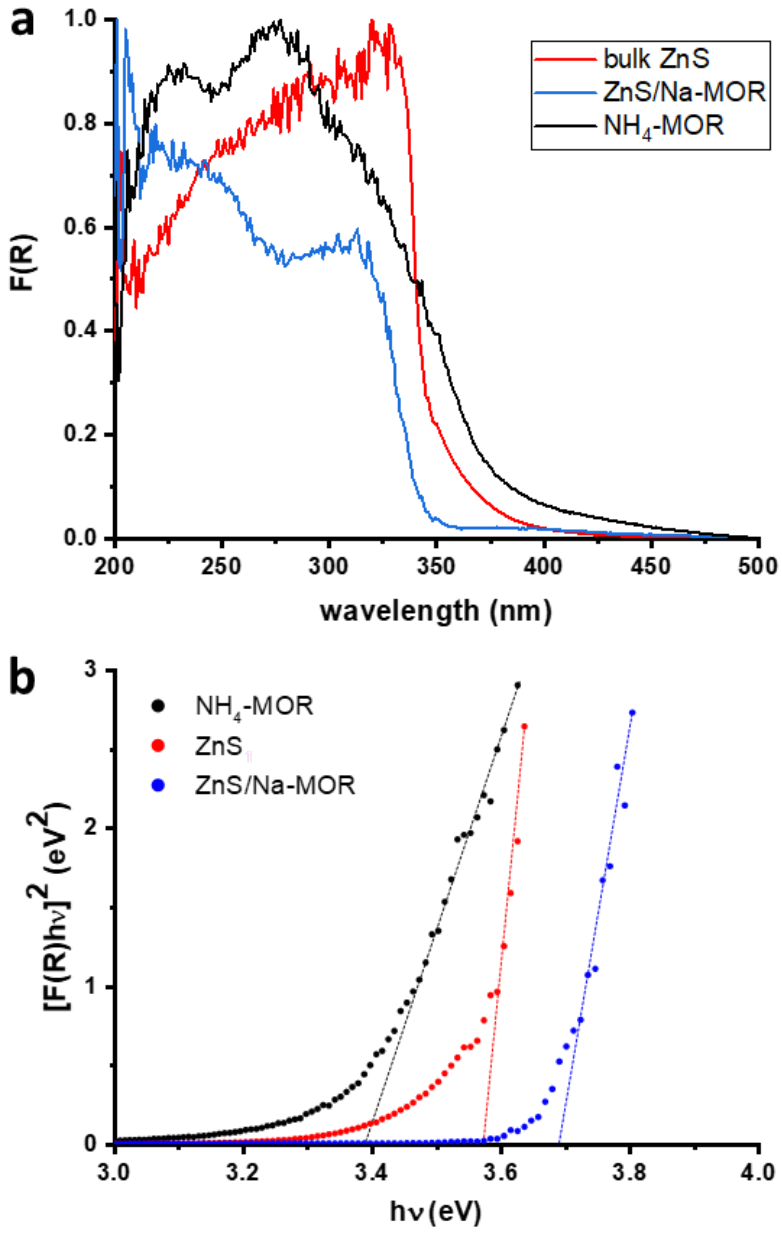

Figure 3: a) Diffuse reflectance UV-Vis spectra (Kubelka-Munk units) of NH_4-MOR (black), bulk ZnS (red), and ZnS/Na-MOR (blue). b) Tauc plot of the Kubelka-Munk function considering that NH_4-MOR (black), bulk ZnS (red), and ZnS/Na-MOR (blue) exhibit direct band gaps.

For evaluating the band gap energies of the compounds obtained here, the Tauc plot was applied considering the Kubelka-Munk UV-Vis data (Figure 3b). [31–33] D'Amico *et al.* used simulations of the electronic structure of the two ZnS crystalline phases to demonstrate that both of them exhibit direct band gaps of 3.25 eV.[34] Here, the experimental value obtained was 3.58 eV, which is close to the reported value for the sphalerite phase (3.6 eV) [35] but lower than the ZnS wurtzite phase (3.8 eV) [36] thus confirming that the sphalerite phase was obtained in ZnS/Na-MOR.

The Kubelka-Munk spectra of both NH_4-MOR and ZnS/Na-MOR exhibit a proper linear region when plotting $[F(R)h\nu]^n$ against $h\nu$ for $n = 2$ – however, this linear region is poorly resolved when $n = ½$. Therefore, the pristine zeolite and the ZnS/Na-MOR composite were also considered to present a direct band gap with energies of 3.39 and 3.69 eV, respectively. The increase of the band gap energy observed after the introduction of ZnS nanoparticles within the zeolite is again ascribed to the quantum size effect that produces a blueshift on the band edge of the bulk ZnS in the UV-vis spectra.[28–30]

To confirm the presence of ZnS nanoparticles, XPS was applied to the ZnS/Na-MOR composite. The main signals observed for this sample and the corresponding atomic ratios are reported in Table 1. Although XPS is considered as a surface analysis technique, the photoelectrons have mean free path around 5 nm in silica/aluminium environment which allows probing the three first channels of zeolite.[37,38] Therefore, the results are supposed, in a first approximation, to be representative of the overall zeolite.

Table 1: XPS data obtained after cationic exchange for the ZnS/Na-MOR samples

Elements	Binding energy / eV	Atoms / unit cell
C 1s	285.0	10.8
O 1s	532.5	77.0
Na 1s	1072.9	7.5
Si 2p	103.0	32.8

Al 2p	74.6	2.5
Zn $2p^{3/2}$	1021.8	4.2
S 2s	226.3	3.7
Zn/S		1.11
Na/Al		1.14
Si/Al		13.16

223

224 The presence of Na 1s (Figure 4a) signal indicates that the cation exchange process successfully replaced the
225 initial NH_4^+ cations of the zeolite by Na^+ because no traces of nitrogen at about 400 eV were detected in the
226 XPS survey spectrum, and sodium elements appear to be in stoichiometric proportion with aluminium
227 (Na/Al ~ 1) as shown in Table 1. In addition, the calcination step under argon of the sample after cationic
228 exchange was reproduced in-situ and followed by FTIR experiments, in which no sign of acidic Brønsted
229 sites at 3650 cm^{-1}, arising from the transformation of NH_4^+ into NH_3 (g) + H^+ upon heating, were observed
230 in the spectrum. Indeed, Na^+ is required into the framework to provide charge neutrality to the negative
231 charge excess caused by the substitution of Si^{4+} by Al^{3+} cations. Moreover, the Zn $2p_{3/2}$ (Figure 4b) and S 2s
232 (Figure 4c) observed respectively at 1022 and 226 eV are similar to those ones found in the literature for
233 ZnS sphalerite phase. [39–41] This feature, in addition to the Zn/S ~ 1 ratio, indicates that ZnS nanoclusters
234 were formed (Table 1).

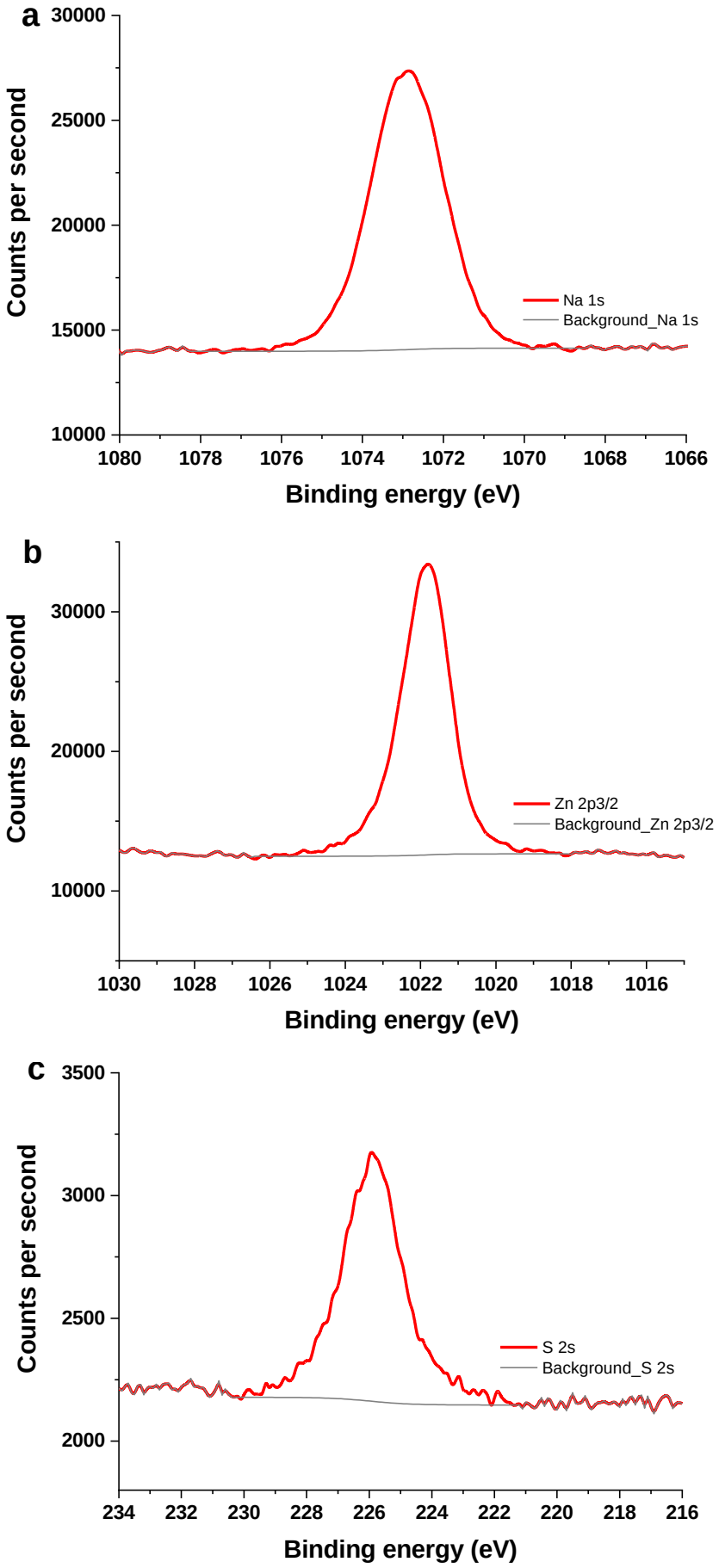

Figure 4: XPS spectra obtained after cationic exchange for the ZnS/Na-MOR sample. (a) XPS signal for Na 1s; (b) XPS signal for Zn $2p_{3/2}$; (c) XPS signal for S 2s

3.2 TRANS-STILBENE ADSORPTION AND PHOTOIONIZATION

Trans-stilbene (*t*-St), a probe molecule with electron-donor character, was adsorbed into the ZnS/Na-MOR composite in order to evaluate the influence of the ZnS nanoparticles upon the charge transfer complexes formed between the Na-MOR and the guest molecules. The incorporation of *t*-St into ZnS/Na-MOR was confirmed by diffuse reflectance UV-Vis spectroscopy (Figure 5a) as shown by the presence of the characteristic absorption band of *t*-St (at λ_{max} = 300 nm) in the spectrum recorded one month after contact between the zeolite and the *t*-St powder. This signal corresponds to *t*-St adsorbed in the porous volume of mordenite zeolite according to Equation (2).

$$t\text{-St} + \text{ZnS/Na-MOR} \rightarrow t\text{-St@ZnS/Na-MOR} \quad (2)$$

It is interesting to note that no spontaneous ionization process was observed after mixing. This feature confirms the efficiency of the elimination of NH_4^+ by cation exchange and the absence of Brønsted acid sites that would be created upon NH_4^+-MOR calcination and acidic H-MOR formation through NH_3 elimination. Indeed, the mere mixing of *t*-St and H-MOR is known to induce spontaneously the formation of radical cation in high amount and its fast subsequent recombination to a charge transfer complex associated with an electron/hole pair. [42]

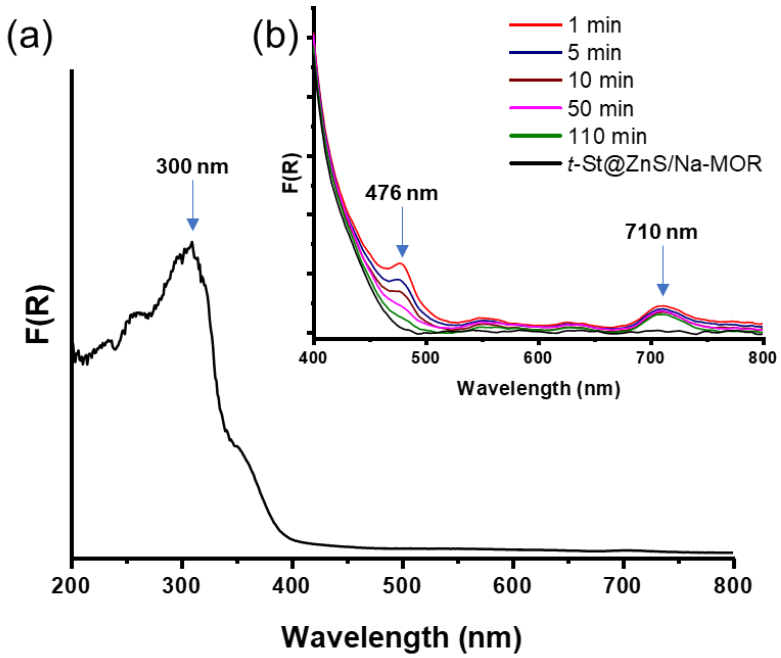

Figure 5: Kubelka-Munk UV−Vis spectrum of (a) *t*-St@ZnS/Na-MOR recorded one month after adsorption before photoexcitation and (b) as a function of time after laser photoirradiation (λ_{ex} = 300 nm).

Thus, the present data are in total agreement with what was observed after incorporating t-St in Na-MOR frameworks where spontaneous ionization of *t*-St was never observed. [6,43] In such case, the guest ionization took place only after photo irradiation. [6] Consequently, by analogy with these previous data, the *t*-St@ZnS/Na-MOR white sample was irradiated using the 300 nm exciting line of a Panther EX OPO pulsed laser as this wavelength falls within the contour of the electronic transition of occluded *t*-St (Figure 3a). After photoexcitation, the sample evolution was followed using conventional diffuse reflectance UV-vis spectroscopy which showed the appearance of two new bands at 477 and 711 nm (Figure 5b). These bands whose intensities decrease with time are characteristic of the *t*-St$^{\bullet+}$ cation radical formation and correspond to transitions $D_2 \leftarrow D_0$ (477 nm) and $D_1 \leftarrow D_0$ (711 nm).[44] The reaction associated to this process is described in Equation (3).

$$t\text{-St@ZnS/Na-MOR} \rightarrow t\text{-St}^{\bullet+}\text{@ZnS/Na-MOR}^{\bullet-} \quad (3)$$

The spectra of *t*-St$^{\bullet+}$@ZnS/Na-MOR$^{\bullet-}$ right after photoirradiation are similar to those obtained during the photolysis of *t*-St in solution, where the lifetime of the radical cation species is in the order of 50 ps.[45]

Moreover, two additional weak absorption bands were observed at about 555 and 615 nm and are attributed to the charge-transfer complex (CTC) between the *t*-St$^{\bullet+}$ cations and the negatively charged ZnS/Na-MOR$^{\bullet-}$ framework, according to Equation (4). [42]

$$t\text{-St}^{\bullet+}@\text{ZnS/Na-MOR}^{\bullet-} \rightarrow t\text{-St@ZnS/Na-MOR}^{\bullet+\bullet-} \quad (4)$$

The guest molecule involvement in the charge transfer is highlighted through the observation of a band structure corresponding to vibronic transitions, as the distances between the maxima are close to 1650-1700 cm^{-1} – approximately the vibrational frequency of the double C=C bond. Indeed, the mechanism of formation of this moiety depends on the oxidizing power of the radical and on the intra-zeolite confinement, as already discussed elsewhere.[6,46,47] The intensities of the bands associated to these charge separate states (*t*-St$^{\bullet+}$ and CTC) decrease progressively in parallel and disappear after more than 110 min, which corresponds to the recombination of the species according to Equations (5) and (6).

$$t\text{-St}^{\bullet+}@\text{ZnS/Na-MOR}^{\bullet-} \rightarrow t\text{-St@ZnS/Na-MOR} \quad (5)$$

$$t\text{-St@ZnS/Na-MOR}^{\bullet+\bullet-} \rightarrow t\text{-St@ZnS/Na-MOR} \quad (6)$$

This behaviour can be compared to that observed previously upon photoexcitation of *t*-St incorporated in Na-MOR.[6] In this previous study, the photoinduced formation of the *t*-St$^{\bullet+}$@Na-MOR$^{\bullet-}$ radical cation was only detected using time resolved diffuse reflectance absorption spectroscopy, with a lifetime of 0.5 s (k = 2.0 s^{-1}). [6] However, it should be noted that in this earlier study with Na-MOR and in the absence of ZnS, the hole transfer and the generation of persistent *t*-St@Na-MOR$^{\bullet+\bullet-}$ moieties reached a lifetime of 2.2 × 10^3 s and was successfully observable using conventional diffuse reflectance UV-vis spectroscopy.

To assess the lifetime of the separate charge states formed in ZnS/Na-MOR and to compare with the lifetimes previously observed after *t*-St photoionization in Na-MOR without ZnS, the concentration decays C(t) of the radical cation generated in ZnS/Na-MOR were fitted according to the Albery function, [48] which takes into account the heterogeneity of the material (Figure 6). The lifetime obtained for *t*-St$^{\bullet+}$ was 18 minutes (k = 0.0553 min^{-1}), which is 10^{14} orders higher than the same cation radical in solution,[49] and about 2 x 10^3 times longer than the lifetime in pristine Na-MOR,[6] and the same timescale as *t*-St@TiO_2-MOR.[7]

Note that the radical cation decay describes two processes that occur simultaneously and in a competitive way: the charge transfer (Equation 4) and the direct charge recombination (Equation 5). Nevertheless, it is not possible to distinguish between both mechanisms.

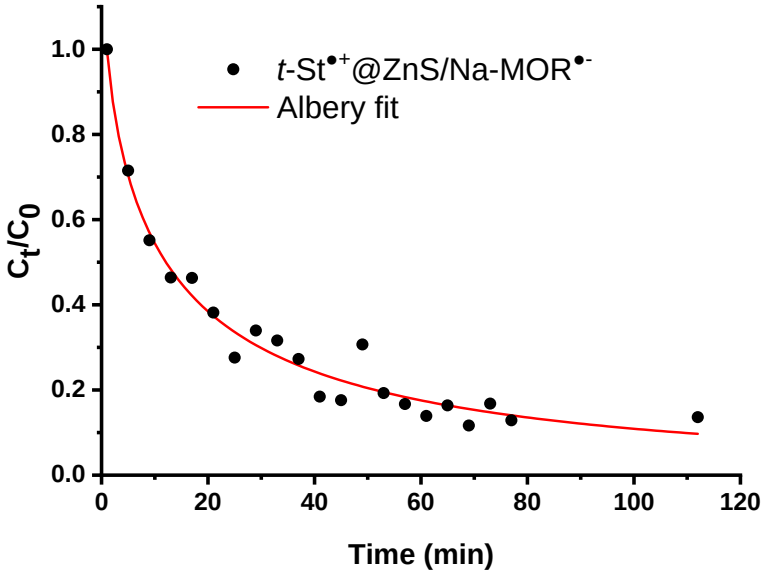

Figure 6: Normalized decay profiles of C_t/C_0 relative to the spectral intensity of *t*-St$^{\bullet+}$@ZnS/Na-MOR$^{\bullet-}$ monitored at 476 nm absorption band after the laser photoirradiation.

As reported above, the presence of the *t*-St$^{\bullet+}$ radical cation was detected by conventional UV-visible spectroscopy in MOR zeolite in the presence of semiconductor nanoparticles.[7] In pristine zeolite, time resolved UV-Vis spectroscopy was necessary to observe its formation.[50] Indeed, the mordenite channel diameter is normally too large and the confinement effect too weak to stabilize the radical cation for a long time.[50] This long lifetime of t-St$^{\bullet+}$ is rather similar to that observed under high confinement in the narrow pores of ferrierite (FER), which induces stabilisation of the radical cation by considerably slowing the kinetics of charge transfer complex (CTC) formation. In the present case, we observe the photoinduced radical cation is clearly detected using classical UV-vis absorption and is much more stable than in pristine Na-MOR. Thus, the *t*-St$^{\bullet+}$ formation and recombination are clearly influenced by the proximity between the guest molecule and the ZnS nanoparticles. Therefore, it is hypothesised that ZnS is also present within the pore channels of the zeolite, which facilitates the capture of the photo-ejected electron by the ZnS conduction band. The stability of the radical also explains why the electron transfer that leads to the charge

transfer complex associated with an electron-hole pair (as observed in Na-MOR) is not favoured in the present case. Nevertheless, it should be noted that the nature of the radical species and the electron transfer mechanisms obtained here are fully consistent with what has been reported previously for a series of zeolites with pores of different opening diameters and for which the reaction intermediates were fully characterised using EPR in addition to UV-vis.

At this point, it is worth discussing the fate of the photo-ejected electron within the zeolite and the process of electron-hole stabilization. The presence of long-lasting cation radicals and CTCs serves as evidence that unpaired electrons can be captured in specific sites, effectively delaying recombination. Previous investigations using pulsed electron paramagnetic resonance (EPR) technique in ZnS-free systems have revealed a correlation between the unpaired electrons and aluminium atoms in the framework, as well as charge-balancing cations.[51] This suggests that electrons are trapped on the oxygen atoms in proximity to aluminium cations.[52] Consequently, the observed phenomenon of non-direct recombination and extended lifetimes may be explained by the occurrence of electron hopping between identical sites within the channels before eventual recombination. In this context, it is plausible to consider the electron's movement from the initial ionization site to subsequent sites before reaching ZnS. As a result, the migration of electrons to ZnS located within the pores or even on the external surface can be envisaged.

4. CONCLUSIONS

ZnS semiconductor nanoparticles were successfully introduced within the porous structure of mordenite and at its surface through a cation exchange process, as demonstrated by the combination of characterisation techniques. The material exhibits a direct band gap of 3.69 eV, which is higher to that of the pristine zeolite (3.39 eV) and bulk ZnS (3.58 eV) due to a quantum size confinement effect. Powder XRD, diffuse reflectance UV-vis spectroscopy, XPS analysis, and HRTEM suggest that cubic ZnS (sphalerite) is the main phase formed in ZnS/Na-MOR. TEM images revealed ZnS nanoparticles of about 3.0 nm anchored to the porous structure of the Na-MOR zeolite, this result is in accord with the particle size estimation from the -XRD pattern using the Scherrer equation. *Trans*-stilbene was successfully adsorbed into the ZnS/Na-MOR

zeolite, as confirmed by diffuse reflectance UV-Vis spectroscopy. After reaching equilibrium, the photoexcitation of the *t*-St@ZnS/Na-MOR sample induced ionization and formation of *t*-$St^{\bullet+}$ cation radical which evolved partially to a charge transfer complexes before recombination. The lifetime of the charged entities evaluated using the Albery model reveals an increase of more than 10^{14} times when comparing to the photolysis of *t*-St in solution (18 minutes in ZnS/Na-MOR, against 50 ps in solution, and 0.5 s in Na-MOR). This is attributed to the proximity between the ZnS semiconductor nanoparticles, also present in the mordenite channels, and the *t*-St probe molecule allowing a charge transfer upon photoionization at 300 nm, as the semiconductor quickly traps the ejected electron and reduces the recombination of the charge carriers. This work provides a direct route for incorporating ZnS semiconductor nanoparticles within the porous structure of mordenite zeolites. The formed composite exhibits improved separation of the charge carriers, reduced recombination, and therefore, allows a more efficient stabilization of charge separated states, which can be interesting for several applications such as photocatalysis, for example.

5. ACKNOWLEDGMENTS

The Chevreul Institute (Surface Analysis facility) is thanked for its help in the development of this work through the ARCHI-CM project supported by the "Ministère de l'Enseignement Supérieur de la Recherche et de l'Innovation", the region "Hauts-de-France", the ERDF program of the European Union and the "Métropole Européenne de Lille.

6. REFERENCES

(1) Erickson, R.; Lund, A.; Lindgren, M. Analysis of Powder EPR and ENDOR Spectra of the Biphenyl Radical Cation on H-ZSM-5 Zeolite, Silica Gel and in CFCl3 Matrix. *Chem. Phys.* 1995, *193* (1), 89–99. https://doi.org/https://doi.org/10.1016/0301-0104(94)00415-7.

(2) Hashimoto, S.; Mutoh, T.; Fukumura, H.; Masuhara, H. Diffuse Reflectance Laser Photolytic Studies of Naphthalene, Biphenyl and Some Aromatic Hydrocarbons Adsorbed in the Cavities of Faujasitic Zeolites. *J. Chem. Soc.{,} Faraday Trans.* 1996, *92* (19), 3653–3660.

https://doi.org/10.1039/FT9969203653.

(3) Ramamurthy, V.; Lakshminarasimhan, P.; P. Grey, C.; J. Johnston, L. Energy Transfer, Proton Transfer and Electron Transfer Reactions within Zeolites. *Chem. Commun.* 1998, No. 22, 2411–2424. https://doi.org/10.1039/A803871F.

(4) Alvaro, M.; García, H.; García, S.; Márquez, F.; Scaiano, J. C. Intrazeolite Photochemistry. 17. Zeolites as Electron Donors: Photolysis of Methylviologen Incorporated within Zeolites. *J. Phys. Chem. B* 1997, *101* (16), 3043–3051. https://doi.org/10.1021/jp9628850.

(5) Moissette, A.; Belhadj, F.; Brémard, C.; Vezin, H. Kinetics and Characterization of Photoinduced Long-Lived Electron–Hole Pair of p-Terphenyl Occluded in ZSM-5 Zeolites. Effects of Aluminium Content and Extraframework Cation. *Phys. Chem. Chem. Phys.* 2009, *11* (46), 11022–11032. https://doi.org/10.1039/B914545A.

(6) Hureau, M.; Moissette, A.; Legrand, A.; Luchez, F.; Sliwa, M.; Bremard, C. Chemical Control of Photoinduced Charges under Confinement in Zeolites. *J. Phys. Chem. C* 2012, *116* (16), 9092–9105. https://doi.org/10.1021/jp301448w.

(7) Legrand, A.; Moissette, A.; Hureau, M.; Casale, S.; Massiani, P.; Vezin, H.; Mamede, A. S.; Batonneau-Gener, I. Electron Transfers in a TiO2-Containing MOR Zeolite: Synthesis of the Nanoassemblies and Application Using a Probe Chromophore Molecule. *Phys. Chem. Chem. Phys.* 2014, *16* (26), 13145–13155. https://doi.org/10.1039/C4CP01543F.

(8) Sarangi, B.; Mishra, S. P.; Behera, N. Advances in Green Synthesis of ZnS Nanoparticles: An Overview. *Mater. Sci. Semicond. Process.* 2022, *147*, 106723. https://doi.org/https://doi.org/10.1016/j.mssp.2022.106723.

(9) Sharma, K.; Raizada, P.; Hasija, V.; Singh, P.; Bajpai, A.; Nguyen, V. H.; Rangabhashiyam, S.; Kumar, P.; Nadda, A. K.; Kim, S. Y.; Varma, R. S.; Le, T. T. N.; Le, Q. Van. ZnS-Based Quantum Dots as Photocatalysts for Water Purification. *J. Water Process Eng.* 2021, *43* (March), 102217. https://doi.org/10.1016/j.jwpe.2021.102217.

(10) Hao, H.; Hu, H.-L.; Liu, Y.; Jiang, F.-L. Trioctylphosphine- and Octanethiol-Induced Photoluminescence Recovery of CdSe/ZnS Quantum Dots after Dilution–Quenching: Implications for

Quantum Dot Films. *ACS Appl. Nano Mater.* 2023, *6* (4), 3085–3094. https://doi.org/10.1021/acsanm.3c00200.

(11) Raymond, O.; Villavicencio, H.; Petranovskii, V.; Siqueiros, J. M. Growth and Characterization of ZnS and ZnCdS Nanoclusters in Mordenite Zeolite Host. *Mater. Sci. Eng. A* 2003, *360* (1), 202–206. https://doi.org/https://doi.org/10.1016/S0921-5093(03)00463-5.

(12) Iacomi, F. Formation of Semiconductor Clusters in Zeolites. *Surf. Sci.* 2003, *532–535*, 816–821. https://doi.org/https://doi.org/10.1016/S0039-6028(03)00446-1.

(13) Wang, Y.; Herron, N. Photoluminescence and Relaxation Dynamics of Cadmium Sulfide Superclusters in Zeolites. *J. Phys. Chem.* 1988, *92* (17), 4988–4994. https://doi.org/10.1021/j100328a033.

(14) Gao, F.; Lu, Q.; Liu, X.; Yan, Y.; Zhao, D. Controlled Synthesis of Semiconductor PbS Nanocrystals and Nanowires Inside Mesoporous Silica SBA-15 Phase. *Nano Lett.* 2001, *1* (12), 743–748. https://doi.org/10.1021/nl0156383.

(15) Álvaro, M.; Carbonell, E.; Atienzar, P.; García, H. A Novel Concept for Photovoltaic Cells: Clusters of Titanium Dioxide Encapsulated within Zeolites as Photoactive Semiconductors. *ChemPhysChem* 2006, *7* (9), 1996–2002. https://doi.org/https://doi.org/10.1002/cphc.200600162.

(16) Patra, S.; Satpati, B.; Pradhan, S. K. Microstructure Characterization of Mechanically Synthesized ZnS Quantum Dots. *J. Appl. Phys.* 2009, *106* (3), 34313. https://doi.org/10.1063/1.3183954.

(17) Hu, J.-S.; Ren, L.-L.; Guo, Y.-G.; Liang, H.-P.; Cao, A.-M.; Wan, L.-J.; Bai, C.-L. Mass Production and High Photocatalytic Activity of ZnS Nanoporous Nanoparticles. *Angew. Chemie* 2005, *117* (8), 1295–1299. https://doi.org/10.1002/ange.200462057.

(18) Andrade, P. H. M.; Gomes, A. L. M.; Palhares, H. G.; Volkringer, C. Post-Synthetic Modification of Aluminum Trimesate and Copper Trimesate with TiO2 Nanoparticles for Photocatalytic Applications. *J. Mater. Sci.* 2022, *57*, 4481–4503. https://doi.org/10.1007/s10853-021-06842-w.

(19) Yitai, Q.; Yi, S.; Yi, X.; Qianwang, C.; Zuyao, C.; Li, Y. Hydrothermal Preparation and Characterization of Nanocrystalline Powder of Sphalerite. *Mater. Res. Bull.* 1995, *30* (5), 601–605. https://doi.org/https://doi.org/10.1016/0025-5408(95)00040-2.

(20) Scherrer, P. Bestimmung Der Größe Und Der Inneren Struktur von Kolloidteilchen Mittels Röntgenstrahlen. *Nachrichten von der Gesellschaft der Wissenschaften zu Göttingen, Math. Klasse* 1918, *1918*, 98–100.

(21) Holzwarth, U.; Gibson, N. The Scherrer Equation versus the "Debye-Scherrer Equation." *Nat. Nanotechnol.* 2011, *6* (9), 534. https://doi.org/10.1038/nnano.2011.145.

(22) Patterson, A. L. The Scherrer Formula for X-Ray Particle Size Determination. *Phys. Rev.* 1939, *56* (10), 978–982. https://doi.org/10.1103/PhysRev.56.978.

(23) Shahi, A. K.; Pandey, B. K.; Singh, B. P.; Gupta, B. K.; Singh, S.; Gopal, R. Photo Physical Studies of PVP Arrested ZnS Quantum Dots. *Electron. Mater. Lett.* 2017, *13* (2), 160–167. https://doi.org/10.1007/s13391-017-6132-7.

(24) Saravanan, N.; Teh, G. B.; Yap, S. Y. P.; Cheong, K. M. Simple Synthesis of ZnS Nanoparticles in Alkaline Medium. *J. Mater. Sci. Mater. Electron.* 2008, *19* (12), 1206–1208. https://doi.org/10.1007/s10854-007-9529-5.

(25) Huo, F.; Wang, Y.; You, C.; Deng, W.; Yang, F.; Pu, Y. Phase- and Size-Controllable Synthesis with Efficient Photocatalytic Activity of ZnS Nanoparticles. *J. Mater. Sci.* 2017, *52* (10), 5626–5633. https://doi.org/10.1007/s10853-017-0797-z.

(26) Rodríguez-Iznaga, I.; Petranovskii, V.; Castillón-Barraza, F. F.; Fuentes-Moyado, S.; Chávez-Rivas, F.; Pestryakov, A. Mordenite-Supported Ag+-Cu2+-Zn2+ Trimetallic System: A Variety of Nanospecies Obtained via Thermal Reduction in Hydrogen Followed by Cooling in an Air or Hydrogen Atmosphere. *Materials (Basel).* 2023, *16* (1) 221. https://doi.org/10.3390/ma16010221.

(27) Geobaldo, F.; Spoto, G.; Bordiga, S.; Lamberti, C.; Zecchina, A. Propene Oligomerization on H-Mordenite: Hydrogen-Bonding Interaction, Chain Initiation, Propagation and Hydrogen Transfer Studied by Temperature-Programmed FTIR and UV-VIS Spectroscopies. *J. Chem. Soc. - Faraday Trans.* 1997, *93* (6), 1243–1249. https://doi.org/10.1039/a607052c.

(28) Norris, D. J.; Bawendi, M. G. Measurement and Assignment of the Size-Dependent Optical Spectrum in CdSe Quantum Dots. *Phys. Rev. B* 1996, *53* (24), 16338–16346. https://doi.org/10.1103/PhysRevB.53.16338.

(29) Yu, J. H.; Joo, J.; Park, H. M.; Baik, S.-I.; Kim, Y. W.; Kim, S. C.; Hyeon, T. Synthesis of Quantum-Sized Cubic ZnS Nanorods by the Oriented Attachment Mechanism. *J. Am. Chem. Soc.* 2005, *127* (15), 5662–5670. https://doi.org/10.1021/ja044593f.

(30) Satoh, N.; Nakashima, T.; Kamikura, K.; Yamamoto, K. Quantum Size Effect in TiO2 Nanoparticles Prepared by Finely Controlled Metal Assembly on Dendrimer Templates. *Nat. Nanotechnol.* 2008, *3* (2), 106–111. https://doi.org/10.1038/nnano.2008.2.

(31) Tauc, J.; Grigorovici, R.; Vancu, A. Optical Properties and Electronic Structure of Amorphous Germanium. *Phys. status solidi* 1966, *15* (2), 627–637. https://doi.org/10.1002/pssb.19660150224.

(32) Tauc, J. Optical Properties and Electronic Structure of Amorphous Ge and Si. *Mater. Res. Bull.* 1968, *3* (1), 37–46. https://doi.org/10.1016/0025-5408(68)90023-8.

(33) Tauc, J. Optical Properties and Electronic Structure of Amorphous Semiconductors. *Opt. Prop. Solids* 1969, 123–136. https://doi.org/10.1007/978-1-4757-1123-3_5.

(34) D'Amico, P.; Calzolari, A.; Ruini, A.; Catellani, A. New Energy with ZnS: Novel Applications for a Standard Transparent Compound. *Sci. Rep.* 2017, *7* (1), 1–9. https://doi.org/10.1038/s41598-017-17156-w.

(35) Jiang, P.; Jie, J.; Yu, Y.; Wang, Z.; Xie, C.; Zhang, X.; Wu, C.; Wang, L.; Zhu, Z.; Luo, L. Aluminium-Doped n-Type ZnS Nanowires as High-Performance UV and Humidity Sensors. *J. Mater. Chem.* 2012, *22* (14), 6856–6861. https://doi.org/10.1039/C2JM15365C.

(36) Díaz-Reyes, J.; Castillo-Ojeda, R. S.; Sánchez-Espíndola, R.; Galván-Arellano, M.; Zaca-Morán, O. Structural and Optical Characterization of Wurtzite Type ZnS. *Curr. Appl. Phys.* 2015, *15* (2), 103–109. https://doi.org/https://doi.org/10.1016/j.cap.2014.11.012.

(37) Dantsin, G.; Suslick, K. S. Sonochemical Preparation of a Nanostructured Bifunctional Catalyst. *J. Am. Chem. Soc.* 2000, *122* (21), 5214–5215. https://doi.org/10.1021/ja994300w.

(38) Gruenert, W.; Schloegl, R.; Karge, H. G. Investigations of Zeolites by Photoelectron and Ion Scattering Spectroscopy. 1. New Applications of Surface Spectroscopic Methods to Zeolites by a High-Temperature Measurement Technique. *J. Phys. Chem.* 1993, *97* (33), 8638–8645. https://doi.org/10.1021/j100135a017.

(39) Dengo, N.; Vittadini, A.; Natile, M. M.; Gross, S. In-Depth Study of ZnS Nanoparticle Surface Properties with a Combined Experimental and Theoretical Approach. *J. Phys. Chem. C* 2020, *124* (14), 7777–7789. https://doi.org/10.1021/acs.jpcc.9b11323.

(40) Onyestyák, G.; Lónyi, F.; Valyon, J. A Study of the Reaction between Zeolite H-Ferrierite and Cd or Zn Metal. *J. Therm. Anal. Calorim.* 2005, *79* (3), 561–565. https://doi.org/10.1007/s10973-005-0579-8.

(41) Bordiga, S.; Turnes Palomino, G.; Pazè, C.; Zecchina, A. Vibrational Spectroscopy of H2, N2, CO and NO Adsorbed on H, Li, Na, K-Exchanged Ferrierite. *Microporous Mesoporous Mater.* 2000, *34* (1), 67–80. https://doi.org/https://doi.org/10.1016/S1387-1811(99)00160-2.

(42) Hureau, M.; Moissette, A.; Vezin, H.; Brémard, C.; Orio, M. Influence of Confinement Effect on Electron Transfers Induced by T-Stilbene Sorption in Medium Pore Acidic Zeolites. *J. Phys. Chem. C* 2012, *116* (2), 1812–1825. https://doi.org/10.1021/jp2065503.

(43) Moissette, A.; Brémard, C.; Hureau, M.; Vezin, H. Slow Interfacial Electron Hole Transfer of a Trans-Stilbene Radical Cation Photoinduced in a Channel of Nonacidic Aluminum Rich ZSM-5 Zeolite. *J. Phys. Chem. C* 2007, *111* (5), 2310–2317. https://doi.org/10.1021/jp066216q.

(44) Majima, T.; Fukui, M.; Ishida, A.; Takamuku, S. Stilbene Radical Anions in the Excited Doublet State. *J. Phys. Chem.* 1996, *100* (21), 8913–8919. https://doi.org/10.1021/jp960282i.

(45) Oberlé, J.; Abraham, E.; Ivanov, A.; Jonusauskas, G.; Rullière, C. Picosecond CARS and Transient Absorption Studies of 1,4-Diphenylbutadiene and Trans-Stilbene: A Study of Photoinduced Formation of a Radical Cation. *J. Phys. Chem.* 1996, *100* (24), 10179–10186. https://doi.org/10.1021/jp960115i.

(46) Hureau, M.; Moissette, A.; Gaillard, J.; Brémard, C. Photoinduced Electron Transfers in Zeolites: Impact of the Aluminum Content on the Activation Energies. *Photochem. Photobiol. Sci.* 2012, *11* (10), 1515–1519. https://doi.org/10.1039/c2pp25121c.

(47) Belhadj, F.; Moissette, A.; Brémard, C. Long-Lived Electron–Hole Pair Formation through Photoionization of Diphenylacetylene Occluded in Medium Pores of Aluminum Rich M6.6ZSM-5 Zeolite (M=Li+, Na+, K+, Rb+, Cs+): Influence of the Counterbalancing Cations on the

Recombination Rate. *J. Photochem. Photobiol. A Chem.* 2009, *208* (2), 203–212. https://doi.org/https://doi.org/10.1016/j.jphotochem.2009.09.016.

(48) Albery, W. J.; Bartlett, P. N.; Wilde, C. P.; Darwent, J. R. A General Model for Dispersed Kinetics in Heterogeneous Systems. *J. Am. Chem. Soc.* 1985, *107* (7), 1854–1858.

(49) Oberlé, J.; Abraham, E.; Ivanov, A.; Jonusauskas, G.; Rullière, C. Picosecond CARS and Transient Absorption Studies of 1,4-Diphenylbutadiene and Trans-Stilbene: A Study of Photoinduced Formation of a Radical Cation. *J. Phys. Chem.* 1996, *100* (24), 10179–10186. https://doi.org/10.1021/jp960115i.

(50) Moissette, A.; Brémard, C.; Hureau, M.; Vezin, H. Slow Interfacial Electron Hole Transfer of a Trans-Stilbene Radical Cation Photoinduced in a Channel of Nonacidic Aluminum Rich ZSM-5 Zeolite. *J. Phys. Chem. C* 2007, *111* (5), 2310–2317. https://doi.org/10.1021/jp066216q.

(51) Vezin, H.; Moissette, A.; Hureau, M.; Brémard, C. Trans-Stilbene Incorporation in Acidic Medium-Pore ZSM-5 Zeolite: A Pulsed EPR Study. *ChemPhysChem* 2006, *7* (12), 2474–2477. https://doi.org/https://doi.org/10.1002/cphc.200600279.

(52) Uliana, M. P.; Pires, L.; Pratavieira, S.; Brocksom, T. J.; De Oliveira, K. T.; Bagnato, V. S.; Kurachi, C. Photobiological Characteristics of Chlorophyll a Derivatives as Microbial PDT Agents. *Photochem. Photobiol. Sci.* 2014, *13* (8), 1137–1145. https://doi.org/10.1039/c3pp50376c.